The Coordination of VO^{2+} to Hydroxamate Binders As Studied by Orientation Selective ESEEM Spectroscopy

V. Kofman,[§] S. A. Dikanov,[+] A. Haran,[§] J. Libman,[†] A. Shanzer,[†] and D. Goldfarb*[,§]

Contribution from the Chemical Physics and Organic Chemistry Departments, Weizmann Institute of Science, Rehovot 76100, Israel, and Institute of Chemical Kinetics and Combustion, Novosibirsk 630090, Russian Federation

Received May 6, 1994[⊗]

Abstract: The binding of VO^{2+} to chiral dihydroxamate binders facilitates the transport of VO^{2+} through the cell membrane into the cell interior, where it was shown to simulate glucose metabolism (Shechter, Y.; Shisheva, A.; Lazar, R.; Libman, J.; Shanzer, A. *Biochemistry* **1992**, *31*, 2063). The unique structure of the binders relies on a modular dipodal topology which generates different binding cavities. The coordination of VO^{2+} to two homologues of these ligands, RL261 and RL239, having different dipod arms but identical donor groups, was investigated by orientation selective electron spin echo envelope modulation (ESEEM) spectroscopy. Relatively deep modulations were observed for the ^{14}N nuclei in the hydroxamate groups in both complexes owing to the fulfillment of the cancellation condition at ~9 GHz. The Fourier transform (FT) ESEEM spectra showed four peaks, three corresponding to the nuclear quadrupole resonance (NQR) lines, ν_o, ν_-, and ν_+, and one to the overtone, $2\nu_m$. In VO-RL261 the NQR and the $2\nu_m$ peaks appear at 1.75, 2.15, 3.9, and 6.0 MHz, respectively, whereas in VO-RL239 they are at 1.75, 2.05, 3.9, and 6.2 MHz, respectively. From the positions of these peaks the ^{14}N quadrupole coupling constant, $|e^2qQ/h|$, the asymmetry parameter, η, and the isotropic hyperfine constant $|a_{iso}|$, were estimated to be 4.0, 0.87, and 2.5 MHz, respectively, for VO-RL261 and 3.8, 0.91, and 2.8 MHz, respectively, for VO-RL239. The unique orientation dependence of the ν_+ peak, which practically disappeared when the field was set to $A_{||}(^{51}V)$, indicates that the principal axis of the quadrupole tensor, z'', is either parallel or perpendicular to the VO axis. In order to obtain more accurate values of the above parameters and to determine the anisotropic hyperfine component, $a_\perp$, as well as the orientations of the hyperfine and quadrupole tensors with respect to the VO axis, a series of simulations were carried out. The best fit parameters showed that $a_\perp$ is rather large (0.6−0.7 MHz) and cannot be neglected and that a_{iso} is smaller than expected, i.e., 1.6−1.8 MHz. We also obtained that z'' is to a good approximation parallel to the VO axis indicating that the two hydroxamate planes are perpendicular to the VO axis in both complexes. Two possible structures, one with a C_2 symmetry, trans configuration, and one with a σ_{xz} symmetry, cis configuration, were considered in the simulations and the latter was found to agree better with the experimental results. The slight differences in the parameters obtained for VO-RL261 and VO-RL239 are attributed to electronic effects induced by the different groups bounded to the hydroxamate carbonyl.

Introduction

Vanadium plays a unique role among biologically relevant ions.[1] One of its special activities is its capability to mimic virtually all functions of insulin such as hexose uptake, glucose oxidation, and lipogenesis both *in vitro*[2−4] and *in vivo*.[5,6] It has also been shown that vanadyl ions,[2,3] rather than vanadate ions, are the biologically active species. Recently, chiral dihydroxamate ligands (Figure 1) were found to effectively bind and transport vanadyl ions across hydrophobic membranes and thereby enhance their biologically activity *in vitro*.[4] The dihydroxamate ligands, all of dipodal topology, were assembled in a modular fashion from homologues dicarboxylates as anchors

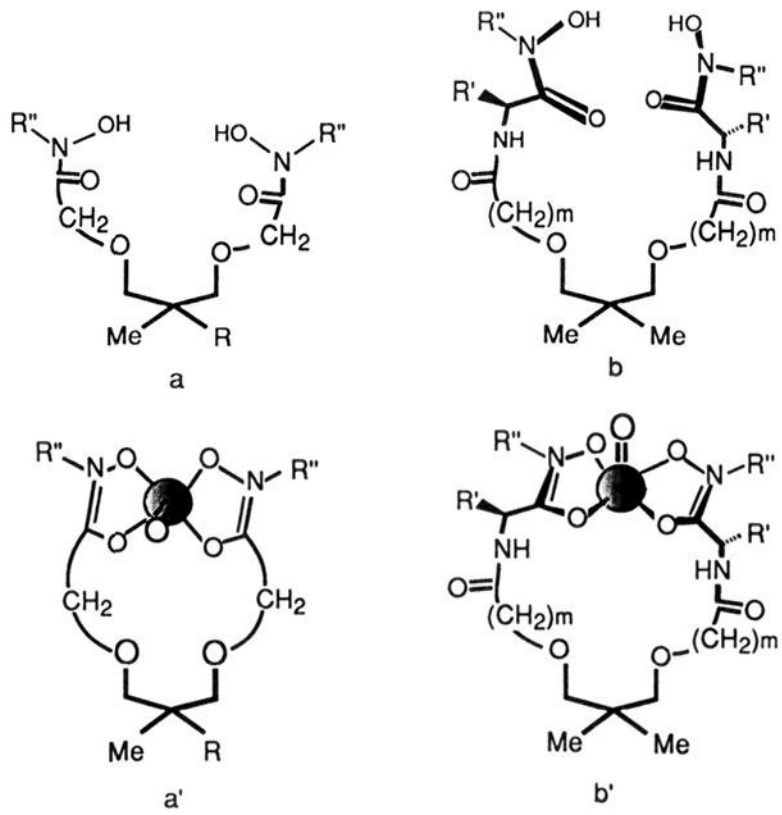

Figure 1. Schematic structures of the ligands studied: (a, a′) RL239 and VO-RL239, R″ = R = Me; (b, b′) RL261 and VO-RL261, R″ = R′ = Me, m = 1.

[§] Department of Chemical Physics, Weizmann Institute of Science.

[+] Institute of Chemical Kinetics and Combustion. Present Address: Macromolecular Structure and Dynamics, Pacific Northwest Laboratories, Richland, WA 99352.

[†] Department of Organic Chemistry, Weizmann Institute of Science.

[⊗] Abstract published in *Advance ACS Abstracts,* December 1, 1994.

(1) Rehder, D. *Angew. Chem., Int. Ed. Engl.* **1991**, *30*, 148. Rehder, D. *Biometals* **1992**, *5*, 3.

(2) Shechter, Y. *Diabetes* **1990**, *39*, 1.

(3) Shechter, Y.; Karlish, S. J. D. *Nature* **1980**, *284*, 556.

(4) Shechter, Y.; Shisheva, A.; Lazar, R.; Libman, J.; Shanzer, A. *Biochemistry* **1992**, *31*, 2063.

(5) Heyliger, C. E.; Tahiliani, A. G.; McNeill, J. H. *Science* **1985**, *227*, 1474.

(6) McMeill, J. A.; Yuen, V. G.; Hoveyda, H. R.; Orvig, C. *J. Med. Chem.* **1992**, *35*, 8.

0002-7863/95/1517-0383$09.00/0

(m = 1 vis. m = 2, Figure 1), chiral amino acids as bridges, and terminating hydroxamate groups as ion binding sites. The modular design and assembly of these compounds enable their systematic modification until optimal performance is achieved. Quite remarkably, pronounced differences were observed in the biological activity of various complexes. For instance, while the family of vanadyl complexes with a backbone with m = 1 (Figure 1) spanned a 20-fold range of activity between the least potent (R′ = Me, alanine) and the most potent (R′ = Bu, phenylalanine) congener, the second family with m = 2 spanned a mere 2-fold range between these extremes.[7]

In order to identify the origin of these differences, information on the structural characteristics, as well as binding and transport properties of the complexes, is required. Since none of the vanadyl complexes has yet been crystallized, we employed spectroscopic methods which provide information on both the spatial and electronic structures of the complexes.

Electron spin echo envelope modulation (ESEEM) spectroscopy is a well-established method for the investigation of binding sites of paramagnetic transition metal ions in orientationally disordered systems.[8-10] It has been found most effective in the case of Cu(II) coordination to imidazole donors in model compounds and in copper enzymes and proteins, where both the hyperfine and the nuclear quadrupole interactions of the remote amino nitrogen were obtained from the ESEEM frequencies.[11-14] The ESEEM effectiveness in these cases is due to the so-called "exact cancellation condition,"[14] which for the remote nitrogen in the Cu(II) imidazole complexes is met at a spectrometer frequency of ~9 GHz. The latter is the frequency at which most of the pulse EPR spectrometers operate.

The three-pulse ESEEM of a paramagnetic center with S = $^1/_2$ coupled to one ^{14}N nucleus consists of six frequencies, three in each m_s manifold. At exact cancellation, the effective field in one of the electron spin manifolds is zero due to the cancellation of the nuclear Zeeman field by the hyperfine field. Therefore, for this manifold the corresponding modulation frequencies are actually the ^{14}N nuclear quadrupole resonance (NQR) frequencies. They appear as narrow peaks in the Fourier-transformed (FT) ESEEM spectrum and their positions are practically independent on the selected magnetic field within the EPR lineshape. Only one of the modulation frequencies corresponding to the other m_s manifold is observed in orientationally disordered systems. It corresponds to the Δm_I = 2 overtone, often referred to as $2\nu_m$. The NQR and the overtone frequencies provide good estimates for the ^{14}N quadrupole coupling constant, e^2qQ/h, the asymmetry parameter, η, and the isotropic hyperfine coupling constant, a_{iso}. The NQR frequencies have been used as fingerprints for the identification of ligands[9,12,15,16] as well as a source for information on the electronic structure.[17] When the EPR spectrum is governed by a large anisotropic interaction, it is possible to perform orientation selective ESEEM experiments. These experiments provide the anisotropic component of the hyperfine interaction and thus a more accurate value for a_{iso}.[18] They also provide the orientation of the ^{14}N hyperfine and quadrupole tensors with respect to the g-tensor which in turn can be interpreted in terms of the complex conformation and bonding characteristics.[18,19]

Vanadyl ions have been successfully employed in the past as spin probes in the investigation of metal binding to proteins. Accordingly, ESEEM has been often used to characterize the VO^{2+} binding to nitrogen-containing ligands in model complexes and to amino acid residues in proteins.[20-23] An obvious advantage of VO^{2+} is its large ^{51}V hyperfine anisotropy which is most useful for orientation selective experiments.[23,24] In most VO^{2+} systems studied so far, the ^{14}N hyperfine couplings were not within the cancellation condition range at X-band. For instance, a_{iso} of the remote ^{14}N in imidazole was recently found to be very small,[25] whereas a_{iso} of the directly bound ^{14}N, 6-7 MHz, is too large.[23,24] An exception is the complex of VO^{2+} with hydrotris(3,5-dimethyl-1-pyrazolyl)borate and dithiocarbamate (LVOdtc), where a_{iso} of the bound ^{14}N is unusually small, 1.7 MHz.[23]

In this work we present orientation selective ESEEM experiments on VO^{2+} complexed with two representative models of the dihydroxamate ligands, RL261 and RL239 shown in Figure 1. The divalent metal cation replaces the two protons and coordinates to four oxygens. The donors in both ligands are the same but the ligands differ in the structure of the dipod arm; the alanine amino acid residue is absent in RL239. We found that the isotropic hyperfine couplings of the ^{14}N nuclei in the hydroxamate units in both complexes fall within the cancellation condition at ~9 GHz, thus providing the means to determine both their hyperfine and quadrupole interactions. Comparison between the two complexes gives information on the effect of the structure and size of the binder on the geometry and electronic structure of the coordination site.

Experimental Section

Ligand Synthesis. The hydroxamate ligands were prepared as described previously.[26] The preparation involved essentially three steps: (i) preparation of the bis(pentachlorophenolates) $Me_2-\{CH_2-OCH_2COOC_6Cl_5\}_2$, (ii) preparation of the aminohydroxamate $H_2-NCHM_eCONOHCH_3$, and (iii) coupling of the phenolates with *N*-hydroxylamine to provide RL239, or coupling of the phenolate with the aminohydroxamate $H_2NCHMeCONOHCH_3$ to provide RL261. Both compounds were purified by column chromatography and were fully characterized by their spectroscopic features, which were in agreement with the assigned structures.

(7) The insulinomimetic effect of the m = 1 series increased from 18 to 90 and 405 for R′ = Me, iBu, and Bu, respectively, while the effects of the m = 2 varies from 58 to 88 and 100 for R′ = Me, Bu, and iBu.

(8) Mims, W. B.; Peisach, J. In *Advanced EPR, Applications in Biology and Biochemistry*; Hoff, A. J., Ed.; Elsevier: Amsterdam, 1989; Chapter 1.

(9) Dikanov, S. A.; Tsvetkov, Yu. D. *Electron Spin Echo Envelope Modulation (ESEEM) Spectroscopy*; CRC Press: Boca Raton, FL, 1992.

(10) *Modern Pulsed and Continuous Wave Electron Spin Resonance*; Kevan, L., Bowman, M. K., Eds.; Wiley: New York, 1990.

(11) Mondovi, B.; Graziani, M. T.; Mims, W. B.; Oltzik, R.; Peisach, J. *Biochemistry* **1977**, *16*, 4198.

(12) McCracken, J.; Pember, S.; Benkovic, S. J.; Villafranca, J. J.; Miller, R. J.; Peisach, J. *J. Am. Chem. Soc.* **1988**, *110*, 1069.

(13) McCracken, J.; Peisach, J.; Dooley, D. M. *J. Am. Chem. Soc.* **1987**, *109*, 4064.

(14) Mims, W. B.; Peisach, J. *J. Chem. Phys.* **1978**, *69*, 4921.

(15) Mims, W. B.; Peisach, J. *J. Biol. Chem.* **1979**, *254*, 4321.

(16) Avigliano, L.; Davis, J. L.; Graziani, M. T.; Marchesini, A.; Mims, W. B.; Mondovi, B.; Peisach, J. *FEBS Lett.* **1981**, *136*, 80.

(17) Jiang, F.; McCracken, J.; Peisach, J. *J. Am. Chem. Soc.* **1990**, *112*, 9035.

(18) Goldfarb, D.; Fauth, J.-M.; Tor, Y.; Shanzer, A. *J. Am. Chem. Soc.* **1991**, *113*, 1941.

(19) Flanagan, H. L.; Gerfen, G. J.; Lai, A.; Singel, D. J. *J. Chem. Phys.* **1988**, *88*, 2162.

(20) Eaton, S. S.; Eaton, G. R. In *Vanadium in Biological Systems*; Chasteen, N. D., Ed.; Kluwer Academic Publishers: Dordrecht, 1990; pp 199-222.

(21) Zhang, C.; Markham, G. D.; Lo Brutto, R. *Biochemistry* **1993**, *32*, 9866.

(22) de Boer, E.; Keijzers, C. P.; Klaasen, A. A. K.; Reijerse, E. J.; Collision, D.; Gamer, C. D.; Wever, R. *FEBS Lett.* **1988**, *235*, 93.

(23) Reijerse, E. J.; Shane, J. J.; de Boer, E.; Collision, D. In *Electron Magnetic Resonance of Disordered Systems*; Yordarov, N. D., Ed.; World Scientific: Singapore, 1989; p 189.

(24) Astashkin, A. V.; Dikanov, S. A.; Tsvetkov, Yu. D. *J. Struct. Chem.* **1985**, *26*, 363.

(25) Dikanov, S. A.; Burgard, C.; Huttermann, J. *Chem. Phys. Lett.* **1993**, *212*, 493.

(26) Shanzer, A.; Libman, J.; Lifson, S. U.S. Patent 5 101 066, 1992; U.S. Patent 5 149 845, 1992.

Sample Preparations. A methanol solution of the ligand (50 μL, 5 mM) was mixed with 12 μL of an aqueous solution of glutathione (20 mM) and then treated under argon with 10 μL of a methanolic solution of $VOSO_4$ (20 mM). The glutathione was added to prevent oxidation of the vanadyl to vanadate. The resulting solution was then transferred into an EPR quartz tube (3 mm o.d.) which was immediately connected to a vacuum line. The solution was then degassed and sealed under vacuum (10^{-4} Torr) at 77 K.

Spectroscopic Measurements. EPR measurements were performed at 140−150 K on a Varian E-12 spectrometer at a frequency around 9.1 GHz. The ESEEM experiments were carried out at 4.2 K and ~9.2 GHz using a home-built spectrometer described elsewhere.[18] The magnetic field and spectrometer frequency were measured with a Bruker NMR gaussmeter (ER-035M) and a HP-5350B frequency counter, respectively. The ESEEM waveforms were recorded using the three-pulse sequence $\pi/2 - \tau - \pi/2 - T - \pi/2 - \tau -$ echo, where the echo intensity is measured as a function of the time interval T. ESEEM waveforms were recorded with τ = 180, 220, and 300 ns. Echo-detected (ED) EPR spectra were recorded using the two-pulse sequence ($\pi/2 - \tau - \pi - \tau -$ echo), where τ is held constant and the echo intensity is measured as a function of the magnetic field. Four-pulse ESEEM waveforms were recorded using the sequence $\pi/2 - \tau - \pi/2 - T/2 - \pi - T/2 - \pi/2 - \tau -$ echo, where the echo is measured as a function of T.[27] The duration of the $\pi/2$ and π pulses was 10 ns, and the amplitude of the π pulse was twice that of the $\pi/2$ pulse. The lengths of the $\pi/2$ and π pulses in the three-pulse ESEEM and in the ED−ESR experiments were 20 ns and 40 ns, respectively. The increment of T was 20 ns, the repetition rate was 100 Hz, and the appropriate phase cycling schemes, eliminating unwanted echoes, were employed.[27,28]

Data Manipulation. To avoid distortions of the FT−ESEEM spectrum due to spectrometer dead time, which for the three-pulse experiment is typically τ + 40 ns, the missing data points were reconstructed using the LPSVD method.[29] Prior to Fourier transformation the background decay was removed either by a polynomial fit or by subtracting the appropriate zero frequency component as obtained from the LPSVD procedure. All spectra shown are the cosine FT−ESEEM.

Basic Equations and Simulations Procedure. The spin-Hamiltonian for VO^{2+} ($S = 1/2$, $I = 7/2$) interacting with two ^{14}N, $I = 1$, nuclei is:

$$\mathcal{H} = \frac{\beta}{h}\vec{H}_0 \cdot \mathbf{g} \cdot \hat{S} + \hat{I} \cdot \mathbf{A}(^{51}V) \cdot \hat{S} + \mathcal{H}_N \qquad (1)$$

The last term includes the ^{14}N nuclear interactions which are usually very small relative to the other interactions and does not affect the EPR spectrum. Therefore, simulations of the EPR spectra were done taking into account only the first two terms, treating the hyperfine terms by second-order perturbation theory,[30] and assuming that the principal axes of $\mathbf{g}$ and $\mathbf{A}(^{51}V)$ coincide.

When the ESEEM is of interest, the nuclear terms ignored above become the most important. The ESEEM can be conveniently calculated once the spin-Hamiltonian in (1) is brought to a block diagonal form such that two nuclear Hamiltonians can be defined and the Mims general expressions can be used.[31]

Diagonalization of the electron Zeeman interaction, neglecting the ^{51}V hyperfine interaction terms,[32] yields the following nuclear Hamiltonians:

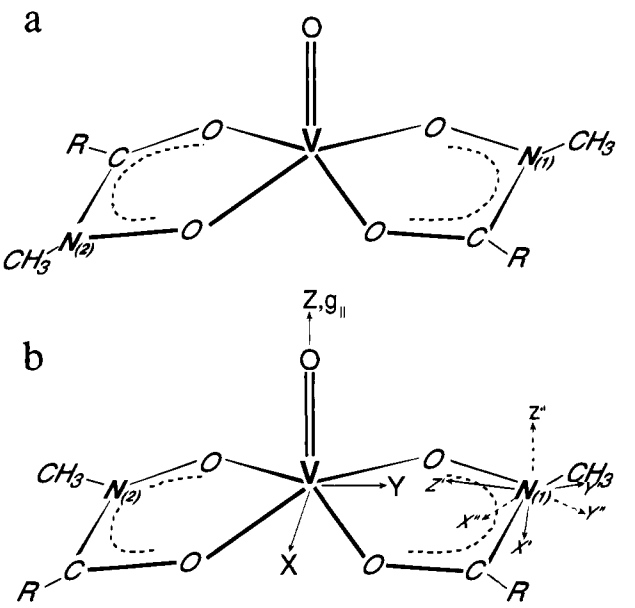

Figure 2. A schematic representation of the hydroxamate binding site and the principal axis systems of the g and $A(^{51}V)$, (X, Y, Z), and the ^{14}N hyperfine (x', y', z') and quadrupole (x'', y'', z'') tensors. The directions of (x', y', z') and (x'', y'', z'') in the figure are arbitrary. Structure *a* possesses a C_2 symmetry (trans), whereas structure *b* has σ_{xz} symmetry (cis).

$$\mathcal{H}_{\alpha,\beta} = \sum_i \left[-\frac{g_n\beta_n}{h}\vec{H}_0 \cdot \hat{I}_i + \hat{I}_i \cdot \mathbf{A}'_i \cdot \hat{S}'_{\alpha,\beta} + \hat{I}_i \cdot \mathbf{Q}_i \cdot \hat{I}_i \right] \qquad (2)$$

A detailed description of the Hamiltonian used is given elsewhere.[18,33,34] The index i denotes the two different nitrogens and $\mathbf{A}'_i = (A^i_{iso} \cdot 1 + \mathbf{A}_i) \cdot \mathbf{g}$,[31,32] where the principal components of $\mathbf{A}$, which is assumed to be axially symmetric, are $-A_\perp$, $-A_\perp$, and $2A_\perp$. For VO^{2+} the g-anisotropy, $\Delta g = g_\parallel - g_\perp$, is small and to a good approximation $\alpha_{iso} = A_{iso}g_{iso}$ and $a_\perp \cong A_\perp g_{iso}$. The principal values of the ^{14}N quadrupole tensor, $\mathbf{Q}$, are:

$$Q^p_{zz} = \frac{e^2qQ}{2h}, \quad Q^p_{xx} = -\frac{1}{2}Q^p_{zz}(1-\eta), \quad Q^p_{yy} = -\frac{1}{2}Q^p_{zz}(1+\eta) \qquad (3)$$

where η is the so-called asymmetry parameter and $|Q^p_{zz}| \geq |Q^p_{yy}| \geq |Q^p_{xx}|$. In the above we omitted the index i for simplicity. The orientation of the external magnetic field, $\vec{H}_0$, with respect to X, Y, Z is given by θ_0 and ϕ_0, and Z was taken along the VO axis which is also the principal axis of the g-tensor. Figure 2 shows a schematic representation of the binding site and the axes systems used. The principal axis systems of $\mathbf{A}'$ (x',y',z') and $\mathbf{Q}$ (x'',y'',z'') are related to that of the ^{51}V hyperfine (X, Y, Z) by the Euler angles 0, θ, ϕ and α, β, γ, respectively.

At exact cancellation, the three-pulse FT−ESEEM spectrum consists of the NQR frequencies, ν_0, ν_-, and ν_+, and the overtone, $2\nu_m$, given by[14,36]

$$\nu_\pm = \frac{3e^2qQ}{4h}\left(1 \pm \frac{\eta}{3}\right), \quad \nu_0 = \frac{e^2qQ}{2h}\eta \qquad (4)$$

and

(27) Gemperle, C.; Aebli, G.; Schweiger, A.; Ernst, R. R. *J. Mag. Reson.* **1990**, *88*, 241.
(28) Fauth, J.-M.; Schweiger, A.; Braunschweiler, L.; Forrer, J.; Ernst, R. R. *J. Magn. Reson.* **1986**, *66*, 74.
(29) Barkhuijsen, H.; de Beer, R.; Bovee, W. M. M. J.; van Ormondt, D. *J. Magn. Reson.* **1985**, *61*, 465.
(30) Ovchinnikov, I. V.; Konstantinov, V. N. *J. Magn. Reson.* **1978**, *32*, 179.
(31) Mims, W. B. *Phys. Rev. B* **1972**, *5*, 2409.
(32) Gerfen, G. J.; Singel, D. J. *J. Chem. Phys.* **1990**, *93*, 4571.
(33) Rowan, L. G.; Hahn, E. L.; Mims, W. B. *Phys. Rev. A* **1965**, *137*, 61.
(34) Goldfarb, D.; Kevan, L. *J. Chem. Phys.* **1987**, *87*, 6323.
(35) Dikanov, S. A.; Yudanov, V. F.; Tsvetkov, Yu. D. *J. Magn. Reson.* **1979**, *34*, 631.
(36) Dikanov, S. A.; Tsvetkov, Yu. D.; Bowman, M. K.; Astashkin, A. V. *Chem. Phys. Lett.* **1982**, *40*, 149.

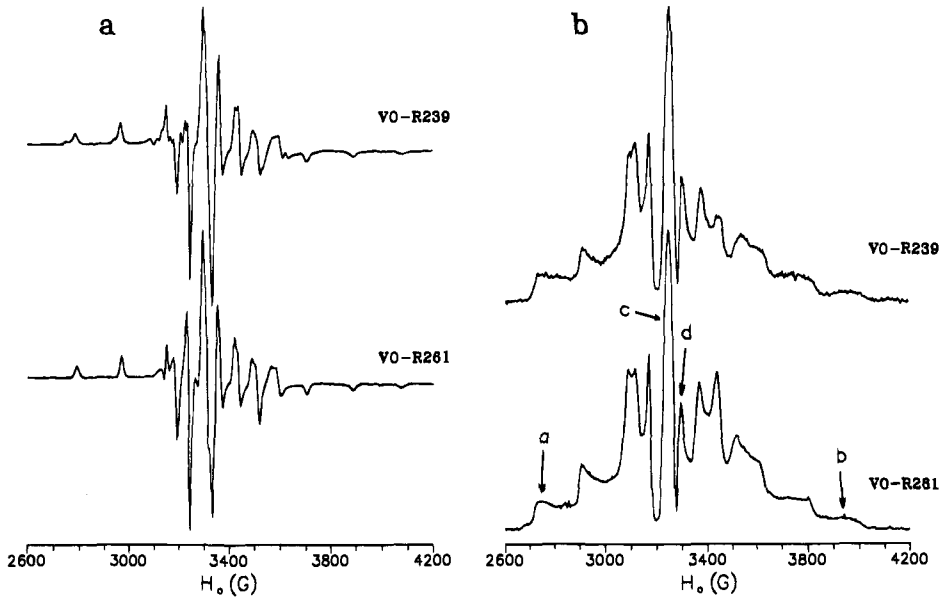

Figure 3. (a) EPR spectra, recorded at 150 K, of methanol solutions of VO-RL261 and VO-RL239. (b) Echo-detected EPR spectra of methanol solutions of VO-RL261 and VO-RL239 recorded at 4 K and $\tau = 0.5$ μs.

$$2\nu_m \cong 2[(\nu_I + a_{iso}/2)^2 + (e^2qQ/4h)^2(3 + \eta^2)]^{1/2} \quad (5)$$

where ν_I is the nuclear Larmor frequency. The expression for $2\nu_m$ was derived under the assumption that the anisotropic hyperfine interaction can be neglected.

The three-pulse echo intensity, $E(T,\tau)$, of a system with $S = {}^1/_2$ and N coupled nuclei, is:[18,35]

$$E(T,\tau) = \int_{\theta_0}\int_{\phi_0}\frac{1}{2}[\prod_i^N E_i^{\alpha}(T,\tau) + \prod_i^N E_i^{\beta}(T,\tau)]f(\theta_0,\phi_0)\sin\theta_0\, d\theta_0 d\phi_0 \quad (6)$$

where $f(\theta_0,\phi_0)$ is a weighting function accounting for the inhomogeneous EPR linewidth and the pulse bandwidth. The ranges of θ_0 and ϕ_0 that contribute to the echo at each magnetic field within the EPR lineshape were determined graphically from plots of the resonance field versus θ_0 for $\varphi_0 = 0°$ and $\varphi_0 = 90°$. The plots were generated through simulations of the EPR spectra where both the ^{51}V hyperfine and the g-anisotropies were taken into account. For each θ_0 a range of 0−180° for φ_0 was taken, neglecting the small biaxiality in $\boldsymbol{g}$ and $A(^{51}\text{V})$. In all simulated FT−ESEEM spectra described above, after removing the "DC" component the time domain patterns were convoluted with a decaying exponent, $e^{-(T/t)}$ (typically $t = 2$ μs), to account for relaxation effects.

Results

Orientation Selective ESEEM Measurements. The low-temperature EPR spectra of VO-RL239 and VO-RL261 in methanol are shown in Figure 3a. The spectra are rather similar, though that of VO-RL239 indicates the presence of an additional minor species. The spectra are characterized by a relatively small g-anisotropy with a negligible biaxiality and a significantly larger anisotropic ^{51}V hyperfine interaction. The $\boldsymbol{A}(^{51}\text{V})$ and $\boldsymbol{g}$ components derived from simulations of the above spectra, ignoring the minor species in the VO-RL239 solution, are listed in Table 1. A sample prepared with glutathione but without the hydroxamate ligand showed a different EPR spectrum, thus indicating that the observed spectrum is of the dihydroxamate complex. Figure 3b presents the echo-detected (ED) EPR spectra of VO-RL261 and VO-RL239. The lowered intensity between turning points in the low-field part of the ED−EPR spectrum could be either due to a modulation effect or to an orientation-dependent phase memory time. The arrows depicted

Table 1. g and $A(^{51}\text{V})$ (10^{-4} cm^{-1}) Values of VO-RL261 and VO-RL239

	g_{xx}	g_{yy}	g_{zz}	g_{iso}	A_{xx}	A_{yy}	A_{zz}
VO-RL261	1.976	1.978	1.940	1.965	60.7	53.4	166.2
VO-RL239	1.976	1.978	1.939	1.964	63.6	55.9	167.2

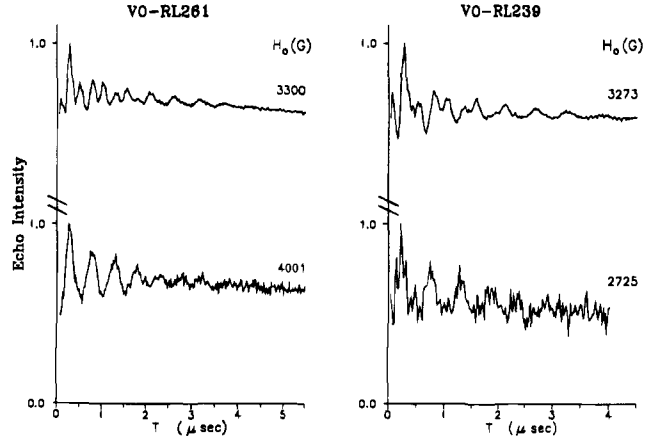

Figure 4. Three-pulse ESEEM waveforms of methanol solutions of (a) VO-RL261 recorded at positions b and d with $\tau = 0.22$ μs. (b) VO-RL239 recorded at position a ($\tau = 0.3$ μs) and position c ($\tau = 0.22$ μs).

on the ED-EPR spectra point at typical positions where the ESEEM experiments were carried out. When the field is set to the most extreme edges of the spectrum (positions a and b, corresponding to the $A_{\parallel}(^{51}\text{V})$ components of the $m_I = \pm{}^7/_2$), only complexes with Z approximately parallel to $\vec{H}_0$ contribute to the echo. Setting the field to position c ($m_I = {}^1/_2$, all possible orientations are selected (isotropic distribution), whereas at position d ($A_{\perp}(^{51}\text{V})$ of $m_I = -{}^1/_2$), all complexes with $Z \perp \vec{H}_0$ are excited (two-dimensional distribution, neglecting the small biaxiality of $A(^{51}\text{V})$).

Typical three-pulse ESEEM waveforms of VO-RL261 and VO-RL239 recorded at positions a and d are depicted in Figure 4. All traces show high-frequency modulation due to protons and deeper, lower frequency modulations due to ^{14}N. FT-ESEEM spectra of VO-RL261 recorded at different magnetic fields for two different τ values, 0.22 and 0.3 μs, are presented

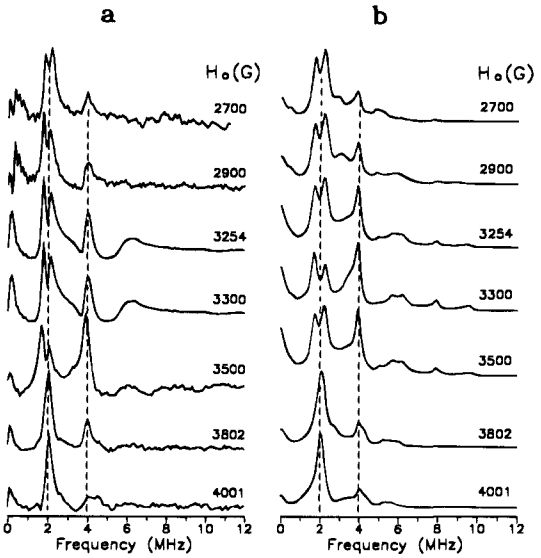

Figure 5. (a) Three-pulse FT−ESEEM spectra of VO-RL261 in methanol as a function of the resonant magnetic field ($\tau = 0.22$ μs). (b) Simulations with the parameters listed in Table 4.

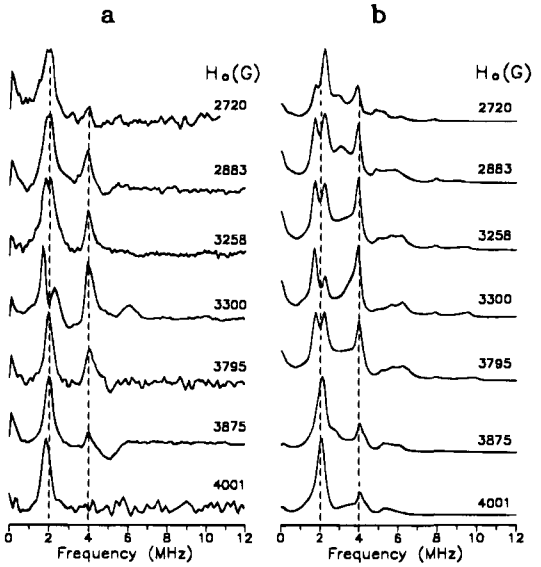

Figure 6. (a) Experimental three-pulse FT-ESEEM spectra of VO-RL261 in methanol as a function of the resonant magnetic field ($\tau = 0.30$ μs). (b) Simulations with the parameters listed in Table 4.

in Figures 5a and 6a, respectively. The spectral region displayed is between 0 to 12 MHz, thus showing only the ^{14}N peaks. All spectra also showed a peak at the protons Larmor frequency, which is outside the range depicted, assigned to weakly coupled protons of the solvent and/or the ligand. The peaks at ~2, 3.9, and 6 MHz are attributed to the ^{14}N nuclei of the hydroxamate donor. Note that at low fields the 2-MHz signal appears as a singlet whereas at higher fields it splits. Most striking is the behavior of the 4-MHz peak; while its position is field invariant, its relative amplitude changes significantly with the field. It is weak at the $A_{||}(^{51}V)$ positions (2700 and 4000 G) and intense at fields within the center of the spectrum. This amplitude modulation is not a consequence of the so-called τ suppression effect[31] since it is present in the two sets of spectra recorded with different τ values. The third broad line at 6 MHz is observable only within a narrow field range, around the center of the spectrum, where almost all orientations contribute to the echo. FT-ESEEM spectra obtained with $\tau = 0.18$ μs were rather similar, also showing a broad weak 6-MHz peak. Based on

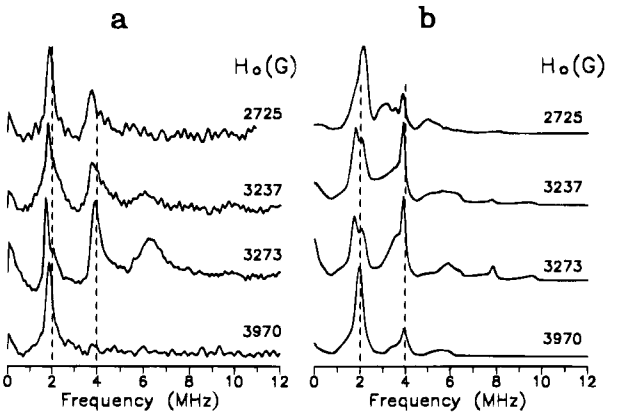

Figure 7. (a) Experimental three-pulse FT-ESEEM spectra of VO-RL239 in methanol as a function of the resonant magnetic field. All spectra were obtained with $\tau = 0.30$ μs except for that recorded at 3317 G (position *c*) which was obtained with $\tau = 0.22$ μs; (b) simulations with the parameters listed in Table 4.

their field dependence, we assign the 1.75; 2.15; and 3.9-MHz peaks to the NQR frequencies ν_0, ν_-, and ν_+ respectively, and the 6-MHz line to the $2\nu_m$ overtone. From the positions of the peaks we estimate (using eqs 4 and 5) that $|e^2qQ/h| \approx 4$ MHz, $\eta \approx 0.87$, and $|a_{iso}| \approx 2.5$ MHz.

The three-pulse FT-ESEEM spectra of VO-RL239, shown in Figure 7a, are generally similar to those of VO-RL261. When recorded at 3273 G (position *c*), it shows NQR peaks at 1.76, 2.1, and 3.86 MHz and a $2\nu_m$ line at 6.3 MHz. These frequencies give $|e^2qQ/h| \approx 4$ MHz, $\eta \approx 0.9$, and $|a_{iso}| = 2.8$ MHz which are slightly different than in VO-RL261. As in VO-RL261, the 1.86-MHz peak is not split and the amplitudes of the 3.8 and 6.2 MHz peaks are significantly reduced in spectra recorded at the $A_{||}(^{51}V)$ positions. The similarity between VO-RL261 and VO-RL239 supports our assignment that in VO-RL261 the VO^{2+} is coordinated to the hydroxamate group and not to the amide group.

In order to rule out the possibility that the ligand is not tetradentate, which would allow the equatorial coordination of solvent molecules (water/methanol), we carried out four-pulse ESEEM experiments on VO-RL261. The measurements were performed at position c with τ values of 250 and 390 ns, optimizing the amplitude of the protons sum harmonic frequency, $2\nu_H$. The four-pulse ESEEM spectra showed only one narrow protons peak (~0.2-MHz width) at $2\nu_H$. A sum combination harmonic peak shifted by 0.8−0.9 MHz from $2\nu_H$, as expected from protons of equatorial water ligands, was not detected.[37] This shows that the VO^{2+} is indeed coordinated to the two hydroxamate groups.

The unique orientation dependence of the ν_+ (4 MHz) peak provides information regarding the orientation of the quadrupole tensor with respect to the principal axis system of $A(^{51}V)$. At exact cancellation the "NQR" peaks are "polarized", i.e., ν_o, ν_-, and ν_+ have maximum amplitudes when $\vec{H}_0$ is parallel to z'', y'', and x'', respectively, and minimum amplitudes when $\vec{H}_0$ is parallel to (x'' or y''), (x'' or z''), and (z'' or y''), respectively.[38] In our specific case the amplitude of ν_+ reaches a minimum at $A_{||}(^{51}V)$; therefore, we conclude that at this orientation $\vec{H}_0 \parallel z''$ or $\vec{H}_0 \parallel y''$, namely, $\beta = 0°$ or $\alpha = \beta = 90°$. Since at both 2700 G and 4000 G the ν_o and ν_- peaks are not well resolved because of the high value of η, clearcut conclusions regarding the orientation dependence of the amplitudes of these two peaks

(37) Tyryshkin, A. M.; Dikanov, S. A.; Goldfarb, D. *J. Magn. Reson. A* **1993**, *105*, 271.

(38) Flanagan, H. L.; Singel, D. J. *J. Chem. Phys.* **1987**, *87*, 5605.

Table 2. Relation between the Euler Angles $\alpha, \beta, \gamma, \theta$, and ϕ of $^{14}N_{(1)}$, and $^{14}N_{(2)}$ for a Trans Configuration (a) and a Cis Configuration (b) of the Hydroxamates Binding Site

	structure a	structure b
$^{14}N_{(1)}$	α, β, γ	α, β, γ
	θ, ϕ	θ, ϕ
$^{14}N_{(2)}$	$\alpha, \beta, \gamma + 180$	$\alpha, 180 - \beta, 180 - \gamma$
	$\theta, \phi + 180$	$180 - \theta, 180 - \phi$

cannot be drawn. Hence, we cannot distinguish the above two options using solely the NQR peaks.

The two possible orientations of z'' can be distinguished through numerical simulation. These would also account for the field dependence of the ν_o and ν_- peaks which are often unresolved at the $A_{||}(^{51}V)$ edges and well resolved at $A_\perp(^{51}V)$. Furthermore, the simulation provides the size and orientation of the anisotropic hyperfine interaction and a more accurate value for the isotropic hyperfine constant.[18,39] Such simulations are presented in the next session.

Simulations. Considering the structure of the ligands, the hydroxamate units can assume two different arrangements, (a) and (b), as shown in Figure 2. In (a) the two nitrogens $N_{(1)}$ and $N_{(2)}$ in units I and II are in a trans configuration, related by a C_2 symmetry axis parallel to the VO axis, whereas in (b) they are in a cis configuration, related by a mirror plane. Table 2 lists the relation between Euler angles, α, β, γ, and θ and ϕ of the two ^{14}N for structures (a) and (b). These were calculated under the assumption that the mirror plane in (b) is along XZ (σ_{xz}). This is a reasonable assumption as the g and $A(^{51}V)$ tensors are nearly axial. The relations given in Table 2 hold as long as the C_2 and σ_{xz} symmetries are not violated. For instance, for both (a) and (b) structures it includes a deviation of the plane of the hydroxamate groups from the plane perpendicular to the VO bond axis through a rotation of units I and II about X by ψ and $-\psi$, respectively. A rotation of both units by ψ about Y breaks the symmetry in (b) but not in (a), whereas a rotation of I and II about Y by ψ and $-\psi$, respectively, keeps the σ_{xz} symmetry in (b) but breaks the C_2 symmetry in (a). The latter distortion is, however, unlikely considering the dipod structure. While we considered different orientations for the quadrupole and hyperfine tensors for the two nitrogens, the amplitudes and signs of the interactions were assumed to be identical. Since we have no experimental results indicating any difference and considering the structure of the ligands, this is a reasonable assumption.

The general effects of the various hyperfine and quadrupole interaction parameters on the ESEEM spectrum under exact cancellation conditions were described in ref 40. In the following we show only a representative series of simulations that outlines the search for the best fit parameters. Table 3 lists the range of θ_0 which was selected at each field as graphically determined using the EPR parameters given in Table 1, and assuming an inhomogeneous line width of ~90 G. In the simulation $f(\theta_0,\phi_0)$ (see eq 6) was taken as a unity. We shall first present the $\alpha = \beta = 90°$ option.

A. $\alpha = \beta = 90°$. Figure 8a shows calculated three-pulse FT-ESEEM spectra for the high-field $A_{||}(^{51}V)$ position (H_0 = 4000 G) and e^2qQ/h = 3.9 MHz, η = 0.87, a_{iso} = 1.6 MHz, and different values of $A_\perp$. In this series of simulations θ was taken rather arbitrarily as 90°, although considering the structure of the ligands it is unlikely that θ is close to zero if we assume that it is dominated by the point dipole interaction. Increasing $A_\perp$ reduces the ν_- intensity and keeps the ν_+ peak intensity

(39) Reijerse, E. J.; Keijzers, C. P. *J. Magn. Reson.* **1987**, *71*, 83.
(40) Goldfarb, D.; Fauth, J.-M.; Farver, O.; Pecht, I. *Appl. Magn. Reson.* **1992**, *3*, 333.

Table 3. Range of θ_0 Selected at Each Field Position

magnetic field, G	^{51}V	θ_0 range
2700	$+^7/_2$	0–33°
2900	$+^7/_2$	54–64°
	$+^5/_2$	0–33°
3254	$+^1/_2$	0–90°
3300	$-^1/_2$	60–90°
3500	$-^3/_2$	35–50°
	$-^5/_2$	55–75°
	$-^7/_2$	75–90°
3802	$-^5/_2$	0–32°
	$-^7/_2$	36–44°
4001	$-^7/_2$	0–33°

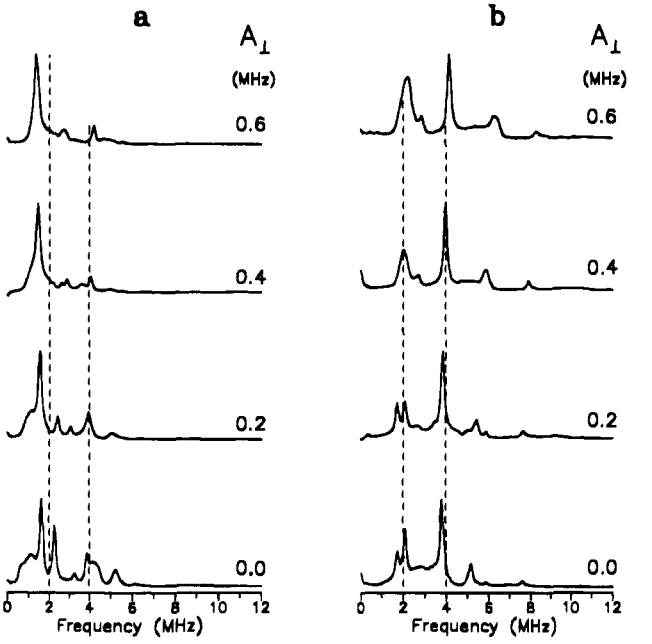

Figure 8. Simulated three-pulse FT-ESEEM spectra showing the effect of $A_\perp$ for (a) the $A_{||}(^{51}V)$ position (H_0 = 40009) and (b) $A_\perp(^{51}V)$ position (H = 3300 G), calculated with the following parameters: e^2qQ/h = 3.9 MHz, η = 0.87, a_{iso} = 1.6 MHz, $\alpha = \beta = 90°$, $\gamma = 0°$, $\theta = 90°$, $\phi = 0°$, and $\tau = 0.3$ μs. Each spectrum is normalized according to its strongest peak; therefore, the amplitudes of the different spectra cannot be compared.

low as in the experimental results. The position of ν_o is, however, somewhat low; a slight increase in e^2qQ/h would shift it toward the experimental frequencies. The effect of $A_\perp$ on the FT-ESEEM recorded at the $A_\perp(^{51}V)$ position (H_0 = 3300 G) is presented in Figure 8b. These spectra also indicate that $A_\perp$ should be between 0.2 and 0.3 MHz. Although the ν_o, ν_- positions in these simulations agree well with the experimental results, their relative intensities do not. Moreover, the position of $2\nu_m$ is slightly shifted from the experimental value. Variations of e^2qQ/h, η, θ, and $(\gamma - \phi)$ did not result in a better agreement. It should be noted that while we could rather easily reproduce the frequency and amplitude dependence of ν_+ and $2\nu_m$, we could not obtain the frequency and amplitude variation of the ν_o and ν_- peaks. The simulated FT-ESEEM spectra were not sensitive to the cis and trans configurations (Figure 2); namely, for the same set of parameters for $N_{(1)}$, similar spectra were obtained for both structures.

B. $\beta = 0°$. Figure 9a shows the dependence of the FT-ESEEM spectrum calculated with e^2qQ/h = 3.9 MHz, η = 0.87, a_{iso} = 1.6 MHz, and H_0 = 3300 G ($A_\perp(^{51}V)$), on $A_\perp$ assuming a trans configuration. A good agreement with the experimental spectra is obtained for $A_\perp$ = 0.2–0.3 MHz. A reasonable agreement is also achieved with a_{iso} = 2 MHz. The dependence

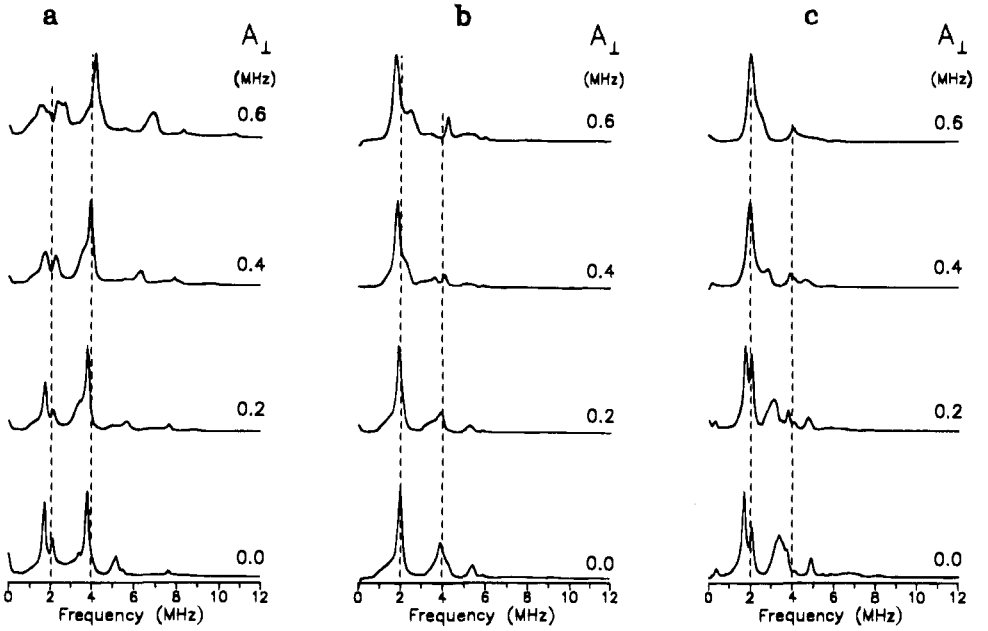

Figure 9. Simulated three-pulse FT-ESEEM spectra showing the effect of $A_\perp$ for (a) $A_\perp(^{51}V)$, H = 3300 G; (b) $A_\parallel(^{51}V)$, H_0 = 4000 G; and (c) $A_\parallel(^{51}V)$, H_0 = 2700 G obtained with the following parameters: $|e^2qQ/h|$ = 3.9 MHz, η = 0.87, a_{iso} = 1.6 MHz, $\alpha = \beta = 0°$, $\gamma = 0°$, $\theta = 90°$, $\phi = 0°$, and τ = 0.3 μs. For (c) τ = 0.22 μs. Each spectrum is normalized according to its strongest peak; therefore, the amplitudes of the different spectra cannot be compared.

Table 4. Best-Fit Parameters[a] Used in Figures 4b and 6b for VO-RL261 and in Figure 7b for VO-RL239

	$\lvert e^2qQ/h\rvert$ (MHz)	η	α^b	β^b	γ^b	α_{iso} (MHz)	$A_\perp$ (MHz)	$\alpha_\perp$ (MHz)	θ^b	ϕ^b
VO-RL261 (Figures 5b, 6b)	4.0	0.84	0	20	0	1.8	0.33	0.65	105	0
VO-RL239 (Figure 7b)	3.8	0.91	0	5	0	1.8	0.40	0.79	110	0

[a] The spectra are actually dependent on $\alpha + \gamma - \phi$, so variations of these angles, keeping $\alpha + \gamma - \phi = 0$, would give similar spectra. [b] Angles in degrees.

of the FT-ESEEM spectra recorded at the $A_\parallel(^{51}V)$ positions (4000 G and 2700 G) on $A_\perp$, calculated with the same parameters, is shown in Figures 9b and 9c, respectively. At these fields, the best agreement is reached when $A_\perp$ = 0.3−0.4 MHz. There are, however, slight disagreements with the experimental results. At 2700 G a peak at ~3 MHz, corresponding to a single quantum ENDOR transition within the manifold where cancellation does not occur, is evident, and at 4000 G the position of the overlapping ν_o, ν_- peaks is slightly shifted to lower frequencies. Nonetheless, this option matches the experimental results better than the $\alpha = \beta = 90°$ case, and we therefore chose it for further refinement of the parameters. As in the $\alpha = \beta = 90°$ case, the simulated FT-ESEEM spectra were practically insensitive to the cis and trans configurations. While the simulations in both options ($\alpha = 90°$ and $\beta = 0°$) were not sensitive to the sign of e^2qQ/h, changing the relative signs of a_{iso} and $A_\perp$ resulted in considerable differences.

Better agreement with the experimental results could be obtained through a refinement of β and θ. Figure 5b shows the simulations of the VO-RL261 spectra at all fields measured for τ = 0.22 μs and $\beta = 20°$. All the other parameters are listed in Table 4, and the selected orientations for each field are given in Table 3. The simulated spectra calculated with the same parameters and τ = 0.3 μs are depicted in Figure 6b. While the simulated FT-ESEEM spectra were not sensitive to the cis and trans configurations, the modulation depth was. Figure 10 shows calculated ESEEM waveforms obtained with the parameters listed in Table 4 for both $A_\parallel(^{51}V)$ and $A_\perp(^{51}V)$. Observation of the ESEEM waveforms in Figure 4 shows that the echo decay due to the electron spin T_1 is rather negligible,

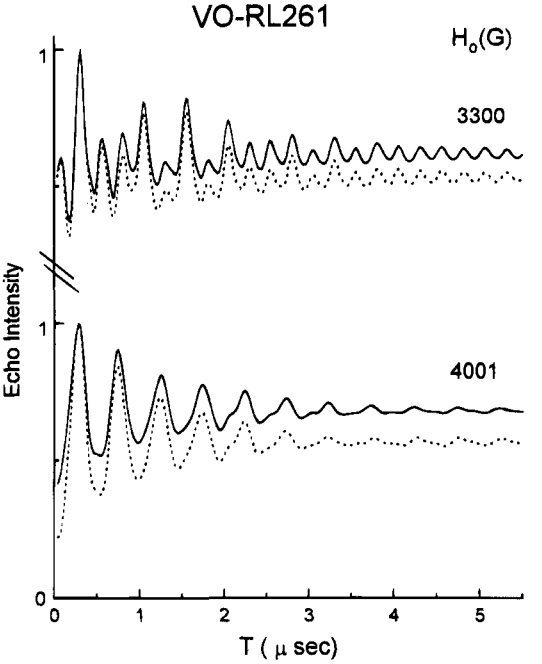

Figure 10. Calculated ESEEM waveforms obtained with the parameters listed in Table 4 for both $A_\parallel(^{51}V)$ and $A_\perp(^{51}V)$ and C_2 (···) and σ_{xz} (—) symmetries.

whereas the simulations showed that the damping of the modulation is significant and stronger than expected solely by the orientational disorder. Thus, additional damping can be attributed to nuclear relaxation and spin diffusion. This was

taken into account in the calculated ESEEM waveforms in Figure 10 by subtracting the constant DC background, multiplying the remaining waveform by a decaying exponent, e^{-T/t_0} (t_0 = 3.0 μs), after which the DC background was readded. This treatment hardly affects the modulation depth at short T which we used as the major feature to be compared with the experimental spectra. The modulation depth for the trans configuration is significantly larger than in the experimental results, especially for the $A_{||}(^{51}V)$ trace. Thus, we conclude that the binding site has a local σ_{xz} symmetry (cis) rather than a C_2 symmetry (trans).

Similar simulations were carried out for VO-RL239. The "best fit" spectra are shown in Figure 7b and the parameters used are listed in Table 4. The parameters are somewhat different from those in VO-RL261; there is a slight decrease in e^2qQ/h and β and a slight increase in η and $A_\perp$. In the case of VO-RL239 we considered only a σ_{xz} symmetry since a C_2 symmetry is not plausible because of steric constraints.

Discussion

Through orientation selective FT-ESEEM spectra of VO-RL261 and VO-RL239, we determined the size and orientation of the ^{14}N hyperfine and quadrupole tensors as given in Table 4. This was done in two stages. First, approximated analytical expressions were used to analyze the field dependence of both the modulation frequencies and amplitudes. These gave good estimates for e^2qQ/h and η, a rough estimate for a_{iso}, and two possible orientations of $\boldsymbol{Q}$. These values were then used as starting points for exact numerical simulations carried out to obtain more accurate values. The simulations showed that the anisotropic hyperfine interaction is significant in these ligands and cannot be neglected if an accurate value for a_{iso} is required. Moreover, it showed that the orientation of $\boldsymbol{Q}$, ($\alpha = \beta = 0°$) is favored over the ($\alpha = \beta = 90°$) option. We also demonstrated that, although the FT-ESEEM spectra can be used to obtain all parameters, it was not sensitive enough to the symmetry of the binding site (trans), C_2, versus σ_{xz} (cis). These could be distinguished by considering the modulation depth in the time domain.

The ^{14}N quadrupole coupling constants and asymmetry parameters of a series of substituted hydroxamic acids were measured by Ruiqin et al.[41] using double resonance field-cycling techniques. The quadrupole coupling constants of the hydroxamate nitrogens in all acids were found to be in the range of 4.6−5.2 MHz and the asymmetry parameters between 0.8 and 1. The high asymmetry parameters, 0.84 and 0.91, we found for VO-RL261 and VO-RL239, respectively, agree well with the above. The quadrupole coupling constants in the VO^{2+} complexes (4.00 and 3.8 MHz) are, however, significantly lower. This decrease may be attributed either to the VO^{2+} binding or to the substitutions of N−H in the hydrodynamic acids by N−CH_3 in the RL261 and RL239 ligands. Substitution on the remote nitrogen in imidazole, however, results in an increase of e^2qQ/h, rather than a decrease along with a decrease in η.[17,42] A similar increase in e^2qQ/h was observed on going from NH_3 to $(CH_3)_3N$.[43] Methyl substitution on the nitrogen bound to an oxygen leading to a small decrease in e^2qQ/h was observed in $[NH_3OH]^+Cl^-$ (4 MHz) and $[CH_3H_2N^+OH]Cl^-$ (3.8 MHz).[44] The above changes caused by substitution on the nitrogen do not support the reduction we observed in e^2qQ/h. The coordination of the VO^{2+} cation to the hydroxamate oxygens is expected to introduce some changes in the electron density at the nitrogens through electronic resonance effects (see Figure 11). This leads to an effective reduction of the electron population in the nitrogen's p_z, where the lone pair resides, owing to its partial participation in a π bond. This in turn may be the cause for the decrease in e^2qQ/h.

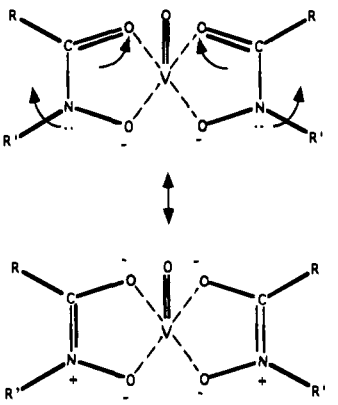

Figure 11. A schematic representation of the resonance in the dihydroxamate binding site.

Ruiqin et al.[41] also performed ab initio SCF−MO calculations on acetohydroxamic acid, acetohyroxamic acid hemihydrate, and oxalidohydroxamic acid to account for the values of e^2qQ/h and η and to predict the orientation of the principal axes of the electric field gradient tensor. Their results indicate that the z'' axis lies in the local π direction, perpendicular to the C−N−H plane, the y'' direction is close to the N−O bond direction, and the x'' axis is in the C−N−O−H plane at an angle of about 30° to the N−H, rotated toward N−O. Our results show that in the two complexes investigated the angle β between the z'' axis and the V−O direction is small. Under the assumption that the metal coordination does not lead to a significant change in the orientation of the local π direction, this implies that the C−N−O plane of the hydroxamate is within a good approximation perpendicular to the VO axis.

In their discussion Ruiqin et al.[41] state that, owing to the large asymmetry parameter, they cannot be absolutely certain that the calculated and experimental Q^p_{zz} indeed correspond to the same axis; namely, the experimentally determined Q^p_{yy} and Q^p_{zz} might have been interchanged. This means that the principal axis of the quadrupole tensor may be along the NO bond. They argued that viewing hydroxamates as a special case of amides, where z'' was found to be perpendicular to the O−C−N plane, supports their assignment of the z'' direction to be along the π direction. Nonetheless, they added that other analogies with compounds having N−O bonds in which z'' was found to be along the N−O disagree with the above. The small value we obtained for β rules out the possibility that z'' is along the N−O axis since this would imply that the VO axis is within the hydroxamate plane which is chemically unreasonable. If z'' were along N−O, then β should have been close to 90°, and, as discussed in the Simulation section, we found this option less likely.

Although the donors in the coordination site of RL239 and in RL261 are identical, subtle differences in their Hamiltonian parameters were detected. The most significant ones are: in VO-RL239, e^2qQ/h is slightly smaller (−0.2 MHz) and η is slightly larger (+0.07) than in VO-RL261. The difference between the two ligands is in their dipod arms which in RL239 lack the alanine amino acid residue. This may lead to both steric and electronic effects. Steric effects may be derived from

(41) Ruiqin, W.; Xiaolan, Y.; Zhenye, F.; Haq, M. M. I.; Khurshid, M. M. P.; Payner, T. J.; Smith, A. S.; Palmer, M. H. *J. Am. Chem. Soc.* **1989**, *111*, 114.
(42) Jiang, F.; Karlin, K. D.; Peisach, J. *Inorg. Chem.* **1993**, *32*, 2576.
(43) Lucken, E. A. C. In *Nuclear Quadrupole Coupling Constants*; Academic Press: London New York, 1969.
(44) Marino, R. A.; Oja, T. *J. Chem. Phys.* **1976**, *56*, 5453.

the shortening of the chain in RL239 which imposes constraints on the binding cavity, and a slight bending of the hydroxamate planes with respect to the VO may occur. The slight changes obtained in β and in $A_\perp$ might indicate differences in steric constraints although the differences are very small and might fall within the experimental error. The electronic effect is due to the different nature of the groups bound to the hydroxamate carbonyl which coordinates to the VO^{2+}. The amide group in RL261 is electron donating, whereas the $O-CH_2-$ in RL239 is electron withdrawing, thereby changing the electron density on the nitrogen. Although these groups are rather remote from the hydroxamate nitrogen, their effect is unambiguously detected as small changes in e^2qQ/h and η. Similar trends were observed in e^2qQ/h and η of the remote nitrogen of substituted imidazoles.[17] Electron-withdrawing substituents at position 4 gave larger e^2qQ/h and smaller η values than those of substituents that "push" electrons. All above differences between VO-RL261 and VO-RL239 are rather subtle and can hardly account for large differences in insulinomimetic activity. It seems thus more plausible that several other factors including the complexes' envelopes determine their activity by influencing the ease by which the active VO^{2+} ion is transferred to the biological recognition sites.

The isotropic hyperfine constant, 1.8 ± 0.2 MHz, is smaller than that of directly coordinated nitrogens (6–7 MHz)[23] and larger than the remote nitrogen in imidazole (0.3 MHz).[25] This is expected since there are only two bonds separating the ^{14}N from the VO^{2+} in the hydroxamate complexes and three bonds in imidazole. This is also manifested in the larger $a_\perp$ we obtained, 0.6–0.7 MHz, compared to 0.26 MHz measured for the remote nitrogen in imidazole.[25] Assuming that the anisotropic hyperfine interaction can be described by the point–dipole approximation, we deduce for a value of $a_\perp = 0.6$ MHz a V–N distances of 2.1 Å. On the other hand, taking the VO bond as 2 Å, the O–N bond as 1.4 Å, and a V–O–N angle of about 120°, we obtain a V–N distance of ~2.8 Å which is significantly larger than that obtained using the point–dipole approximation. This indicates that the latter is not valid and that the anisotropic hyperfine interaction contains a significant contribution from spin population in the p orbital. This is in agreement with results obtained from a series of Cu(II) complexes with substituted imidazoles which showed that $a_\perp$ of the remote nitrogen varied from 0.08 to 0.23 MHz depending on the substituent.[17]

Finally, a comment regarding the orientation of the hyperfine tensor, the simulation gave the best fit parameters at $\theta = 105 - 110°$ and $\alpha + \gamma - \phi = 0°$ indicating that z' is not along the V–N axis. This is not surprising as we already mentioned that the point–dipole approximation is not valid and that $a_\perp$ is affected significantly by the spin density transferred from the VO onto the ligands. A large deviation (~40°) from the Cu–N (remote) axis was also observed in a single crystal of Cu(II)-doped zinc bis(1,2-dimethylimidazole) dichloride.[45]

Conclusions

In the VO-RL261 and VO-RL239 complexes the vanadyl coordinates to four oxygens, two in each of the hydroxamate groups. The ^{14}N isotropic hyperfine constant, 1.8 ± 0.2 MHz, is approximately twice the ^{14}N Larmor frequency at ~9 MHz, thus fulfilling the cancellation condition. This enabled the determination of the NQR frequencies from which the quadrupole coupling constants (3.8, 4.0 MHz) and the asymmetry parameters (0.84, 0.91) were obtained, respectively. Orientation selective ESEEM experiments provided the size (0.6–0.7 MHz) and orientation of anisotropic hyperfine interaction and the orientation of the ^{14}N quadrupole tensor. From the latter it was concluded that in both complexes the hydroxamate plane is perpendicular, to within 20°, to the VO axis and that the two hydroxamate groups are in a cis configuration rather than a trans configuration. Slight differences in e^2qQ/h and η were detected between VO-RL261 and VO-RL239 and attributed to electronic effects induced by the alanine residue in the dipod chain of RL261.

Acknowledgment. This research was supported by the Israel Science Foundation administered by the Israel Academy of Science and Humanities. S.A.D. thanks the Department of Chemical Physics of the Weizmann Institute of Science for supporting his stay at this Institute and for the hospitality shown. We thank Dr. D. van Ormondt for giving us the LPSVD computer program.

JA941390Q

(45) Colaneri, M. J.; Potenza, J. A.; Schungar, H. J.; Peisach, J. *J. Am. Chem. Soc.* **1990**, *112*, 9451.